Journal of Materials Science: Materials in Engineering

ORIGINAL PAPER Open Access

Phase stability and tensile properties of metastable β-Ti alloys for orthopedic applications designed using electronic parameters

Nthabiseng Abigail Moshokoa[1*], Mamookho Elizabeth Makhatha[1*], Lerato Raganya[2], Nkutwane Washington Makoana[3] and Maje Phasha[4]

Abstract

The design and development of metastable β-Ti alloys with non-toxic elements that are used in the manufacturing of orthopedic implants are gaining significant research attention. In this work, two metastable β-Ti alloys, binary alloy of Ti-17Mo wt% (referred as Alloy A) and ternary alloy of Ti-16.5Mo-1.1Fe wt% alloy (referred as Alloy B) were designed with different values of electronic parameters such as the Molybdenum equivalence (*Moeq*), electron to atom ratio (*e/a*), and the *Bo-Md*. The contribution of the electronic parameters in influencing the formation of phases and the elastic modulus is discussed. Phase characterization and tensile properties of the alloys after solution treatment at 1100 °C and quenched in ice-brine were carried out using different techniques. The X-ray diffraction (XRD) patterns and optical microscopy (OM) micrographs showed that with increasing *e/a* ratio the β phase stability increases. EBSD phase maps showed the decrease in the volume fractions of α″and ω phases upon addition of Fe. With increase in stability of β phase, the ultimate tensile strength (UTS) and elastic modulus decreased from 912 MPa to 540 MPa and 82 GPa to 73 GPa in Alloy A and Alloy B, respectively. On the other hand, the increase in the β phase stability resulted in increased hardness from 366 $Hv_{0.5}$ for Alloy A to 428 $Hv_{0.5}$ in Alloy B. Using scanning electron microscopy (SEM), a combination of cleavage facets and dimpled structure were observered in both alloys.

Keywords Ti-Mo-Fe alloys, *e/a* ratio, Moeq, X-ray diffraction, Elastic modulus, Ultimate tensile strength

*Correspondence:
Nthabiseng Abigail Moshokoa
Nthabisengmoshokoa@gmail.com
Mamookho Elizabeth Makhatha
emakhatha@uj.ac.za
[1]Department of Metallurgy, School of Mining and Metallurgy and Chemical Engineering, University of Johannesburg, Doornfontein Campus, Johannesburg, South Africa
[2]Advance Materials Engineering, Manufacturing Cluster, Council for Scientific and Industrial Research, Meiring Naude Road, Brummeria 0184, Pretoria, South Africa
[3]National Laser Center, Council for Scientific and Industrial Research, Meiring Naude Road, Brummeria Pretoria 0184, South Africa
[4]Physical Metallurgy Group, Advanced Materials Division, 200 Malibongwe Drive, Mintek, Randburg 2125, South Africa

Introduction

A metallic biomaterial is a material or a combination of materials, which is either natural or artificial in origin that is employed for a duration of time or as a component of a system to heal, improve, or replace the specific human body tissue or any organ or the natural functioning of the body (Todros et al. 2021). Due to its benefits, such as superior mechanical properties such as yield strength, ductility, fatigue strength, and fracture toughness, metallic biomaterials are used to fabricate orthopedic implants such as joint replacement prosthetic, heart valves, tooth fixation in dental implants, manufactured ligaments and tendons, blood vessel prostheses, bone plates, bone cement, cochlear replacements, skin repair devices and contact lenses (Tathe et al. 2010). Amongst the group of various metallic materials, titanium (Ti) and its alloys, mostly Ti6Al4V alloy, are currently being widely used for manufacturing orthopedic implants because of their excellent bio-compatibility, corrosion resistance, high strength-to-weight ratio and low elastic modulus compared to other metallic biomaterials (Okazaki et al. 1998; Zhou et al. 2005). Regardless of its outstanding properties, Ti6Al4V alloy possesses two major drawbacks that challenge its further use as a biomaterial. The first drawback is the release of toxic elements of vanadium (V) and aluminium (Al) from the parent material to the human body that are associated with health issues, and the other drawback is the high elastic modulus of 110 GPa which is much higher as compared to the human bone which is between 10 and 40 GPa (Sakaguchi et al. 2005; Liang 2020; Cui et al. 2024). The mismatch in the elastic modulus between the human bone and the implant results in bone atrophy which eventually leads to implant failure (Zhang and Chen 2019). The above reasons have motivated the focus on the design and development of metastable β-Ti alloys that have non-toxic elements such as Ta, Nb, Mo, Sn, etc., with moderate to high strength and low elastic modulus (Cui et al. 2024). Long-term implants have certain requirements that the candidate material should meet, e.g. the candidate material should be compatible with the surrounding living tissue and the bone in terms of mechanical biocompatibility for example. Cui et al. reported that the mechanical properties of a material is influenced by its processing technique, its phase or crystal structure and microstructure constituents. Therefore, it is very vital that when designing metastable Ti alloys attention is carefully paid into the formation of phases and microstructure. Alloy design refers to the process of selecting proper compositions of a suitable alloying elements and subjecting them to specific heat treatment or thermo-mechanical process to obtain the alloy that meets the application needs (Cui et al. 2024).

Up to now, some studies correlating to mechanical performance to the microstructure have be conducted on binary Ti-Mo alloys (Wang et al. 2016). The process of solution heat treatment which is followed by water quenching can result in formation of metastable phases such as such as hexagonal martensite α′ (Oliveira et al. 2007), orthorhombic martensite α″ (Alves and Rezende 2017; Davis and Flower 1979), and athermal omega (ω) phase (Min et al. 2015). Based on the Mo content, the following phase formation sequence is reported: $\beta \rightarrow \alpha'$ ($0 < x \leq 6$ wt%), $\beta \rightarrow \alpha''$ ($6 < x \leq 8$ wt%) and $\beta \rightarrow \omega$ ($x > 8$ wt%) (Samimi et al. 2014). In recent years, Ti-Mo alloys as potential biomaterials have been studied with the emphasis on their microstructure and mechanical properties. Molybdenum in titanium alloys can improve corrosion resistance, help reduce elastic modulus and enhance ductility (Oliveira et al. 2007). Several studies are reported in literature on Ti-Mo alloys, demonstrating better biocompatibility because Mo can lower the elastic modulus effectively by stabilizing β phase, it is biocompatible and non-toxic element (if added within acceptable concentration) and it is cheaper as compared to Nb and Ta. In terms of mechanical compatibility, the following studies were reported: Studies by Ho et al. and Zhao et al. reported that the amount of ω phase is formed in Ti-xMo alloys when the high Mo content is between 10 and 12 wt% and decreases as the Mo content increases ($10 \leq x \leq 20$ wt%) (Ho et al. 1999; Zhao et al. 2012a, b; Ho 2008). Ho et al. evaluated the microstructure and tensile properties of as-cast Ti-xMo alloys ($x = 7.5$ and 15 wt%). Their light optical microscope showed fine, acicular martensitic (α″) morphology in Ti-7.5Mo and the retainment of β phase with a significant amount of equiaxed morphology in Ti-15Mo alloy. They reported an ultimate tensile strength (UTS) of 1019 MPa, yield strength (YS) of 737 MPa and elastic modulus of 70 GPa in Ti-7.5Mo alloy whereas in Ti-15Mo alloy, the UTS was lower at 921 MPa, while YS and E were higher at values of 745 MPa and 84 GPa, respectively (Ho 2008). Moshokoa et al. investigated the bending properties of solution treated Ti-xMo alloys ($x = 10$, 12.9 and 15 wt%) designed using theoretical methods such as molybdenum equivalence, and electron to atom (*e/a*) ratio. Presence of the α″ in Ti-10Mo was observed, resulting to bending strength of 1552 MPa and high bending modulus of 97 GPa. On the other hand, the β phase was observed in Ti-12.9Mo and Ti-15Mo alloys with bending strength of 1500 MPa and 1627 MPa, and bending modulus of 84 GPa and 74 GPa, respectively (Moshokoa et al. 2022). The release of metallic ions in the human body is caused by low wear and corrosion resistance, which they are considered to be responsible for reported toxic allergies in the human body (Bălţatu et al. 2015). Literature studies on corrosion resistance of Ti-Mo alloys continue to be a subject

of investigation. For example, Oliveira and Guastaldi investigated the electro-chemical behavior of pure Ti and Ti–Mo alloys (6–20 wt% Mo) (Oliveira and Guastaldi 2009). Rezende et al. evaluated the effect of three commercial mouthwashes on the corrosion resistance of Ti–10Mo alloy. Their results demonstrated that Ti–10Mo alloys can be applied for orthopedic devices. Although Ti–10Mo alloys have been found to possess superior corrosion resistance compared to Ti–Ni alloys, with Mo being a favoured non-toxic alloying element, Ti–10Mo alloy has not yet been used as a biomaterial in bone tissue engineering (Alves Rezende et al. 2007). Another study, Wei et al. revealed Ti-16Mo showed potential to to be considered for bone-tissue application because its corrosion rate increased about 100 times when it was investigated for wear and corrosion properties in a phosphate buffered saline by a ball-on plate tribometer (Xu et al. 2020a, b). The effects of Mo content on the corrosion and tribo-corrosion behaviors of Ti-xMo (x = 8, 10, 12, 14, 16, and 20 wt%) alloys fabricated by powder metallurgy were investigated by Xu et al. (Xu et al. 2020a, b). Their results showed that Ti-16Mo alloy exhibited highest Vickers hardness of 403 Hv, whereas the XRD patterns revealed peaks belonging to β phase and acicular α phase, leading to the alloy exhibiting the lowest wear rate as opposed to other alloys despite the tribo-corrosion resistance being the highest (Xu et al. 2020a, b). Zhao et al. developed a new Ti-Mo alloy with changeable Young's modulus for spinal fixture devices by subjecting Ti-16Mo alloy through different thermo-mechanical processing (hot rolling + solution treatment and cold rolling). Presence of peaks belonging to only β phase were observed after hot rolling and solution treatment whereas peaks of β + ω phase were revealed after cold rolling. An increase in hardness after solution treatment (255 Hv) and after cold rolling (266 Hv) was reported. Young's modulus was recorded to be 75 GPa after solution treatment and 87 GPa after cold rolling (Zhao et al. 2012a, b). Luo et al. examined the microstructure, thermo-mechanical properties and Portevin-Le Chatelier effect in Ti-xMo (x = 10, 12, 15 and 18 wt%) alloys using TEM technique and Gleeble 3500 testing machine. Their results showed that Ti-18Mo alloy possessed low yield strength and elastic modulus due higher volume fraction of β phase and reduced ω phase (Luo et al. 2019).

From the above literature, it is clear that the developed alloys were able to retain the β phase, while others experienced precipitation of the ω phase which affected their mechanical properties, more especially the elastic modulus. The literature studies above have demonstrated the compatibility of Mo in terms of its good corrosion resistance. However, from mechanical compatibility point of view, the strength of investigated Ti-Mo binary alloys with high Mo content such as Ti-16Mo (700 MPa), Ti-17Mo (750 MPa) and Ti-18Mo (800 MPa) reported in literature are insufficiently less 1000 MPa, a factor that poses a challenge for their intended use in biomedical applications, e.g. load bearing implants. Therefore, there is still a need for developing more new alloys that can match Ti-6Al-4 V alloy in terms of strength and remain compatible and cost-effective (Abdel-Hady Gepreel and Niinomi 2013). Therefore, researchers have focused more attention on developing low-cost Ti alloys for biomedical applications using common elements while minimizing the content of high-cost rare elements such as Nb, Ta, etc. (Abdel-Hady Gepreel and Niinomi 2013).,. For example, Ti-(10–12)Cr (Zhao et al. 2012a, b), Ti-10Fe-10Ta (Haghighi et al. 2015), and TMF55 (Abd-elrhman et al. 2016) have been recently developed. whereas adding iron to a titanium alloy can enhance its strength (Liu et al. 2006). Moreover, the presence of Fe as a second alloying element in these alloys developed, even in small amount, could have an impact on the corrosion resistance and, possibly, on their biological performances (Min et al. 2010; Niu et al. 2021). As already evidenced for the family of alloy studied, Fe was chosen due to its low cost, strong β stabilization effect and effectiveness in solid-solution strengthening (Catanio Bortolano et al. 2022),. It has been reported that Ti-3Fe binary alloy could present an ultrahigh strength of 1300 MPa after simple heat treatment (Sandlöbes et al. 2019). While the porous Ti88.2Fe11.8 (at%) manufactured by liquid metal dealloying presenting an extremely low elastic modulus as 4.5 GPa with 568 MPa maximum strength (Okulov et al. 2018). A study by Niu et al. revealed that corrosion resistance of Ti-xFe (x = 0, 0.2, 0.5, 1, 2,3 and 4 wt%) was higher due to grain refinement of Fe addition, the passive film formed over the β phase were containing more Fe oxides. Ti-2Fe alloy showed the highest corrosion resistance due the balance in the grain refinement (Niu et al. 2021).

Metastable β-Ti-Mo-Fe alloys have been and are continuously being explored, either designed using the trial and error method and evolving to using other design methods such as the theoretical predictive methods or electronic parameters. For instance, Lin et al. investigated the effect of Fe addition on the alloy structure and mechanical properties of as-cast designed using the trial and error method Ti-7.5Mo-xFe (x = 0, 1–7 wt%). They reported a combination of β + α″+ω in low Fe content and retainment of the β phase from 2 to 5 wt%. Above the 5 wt% Fe they reported the formation of dendritic structures (Lin et al. 2002). In another study, Kobayashi et al. revealed the effect of Fe addition on the microstructure formation and mechanical properties of as-quenched Ti-2.0Mo-xFe (x = 0.5, 1, 1.5 and 2 at%) → Ti-3.93Mo-xFe (x = 0.573, 1.15, 1.72 and 2.29 wt%) and Ti-3Mo-xFe (x = 0.5, 1, and 1.5 at%) → Ti-5.84Mo (x = 0.57, 1.13 and

1.70 wt%). The formation or presences of phases included the β + α″ in alloy with low Fe content, as the Fe content increased the α″ phase was no longer visible and the formation of β + ω was more pronounced. The elastic modulus in both alloys increased significantly with an increase in Fe content. The study does not report on the design method to attain the compositions, therefore their design methods can be concluded as unknown. The alloys did not retain the β phase, however the formation of the precipitation of the ω phase affected the elastic modulus significantly by increasing it (Kobayashi et al. 2014). There are studies that used theoretical methods to design their compositions and also to predict the formation of phases in those alloys. For example, Abd-elrhman et al. investigated the compatibility and performance of new low cost β-type Ti alloys (Ti-4.7Mo-4.5Fe at% →Ti-8.9Mo-4.99Fe wt%) using the *Bo* and *Md* method, where the alloy was predicted to be situated within the martensitic region. The hot rolled and solution treated alloy depicted β + α″ phase with a young's modulus of 83GPa and ultimate tensile of 974MPa (Abd-elrhman et al. 2016). Abd-elrhman et al. presented two β + α type Ti alloys (Ti-2Mo-0.5Fe at% → Ti-5.8Mo-0.57Fe wt%) and (Ti-3Mo-0.5Fe at% → Ti-3.9Mo-0.57Fe wt%) which were designed using the *Bo* and *Md* method as potential low-cost Ti alloys for biomedical applications. The alloys were hot rolled and then subjected to solution treatment showed a combination of β + α″ phase with a decrease in elastic modulus from 84 GPa to 82 GPa, tensile strength of 949 MPa to 800 MPa (Abdelrhman et al. 2019a, b).

The studies in literature showing positive progress reported alloys designed using both the theoretical predictive and trial-and-error methods, however the alloys reported in the published studies possesses low content of Mo that might still pose challenges in the stabilization of the β phase, hence the presence of the α″ and some the precipitation of the ω phase were observed in the results. The addition of Fe content differs in some alloys however high content of Fe can pose challenges in the formation of B2 intermetallic brittle phase, thus careful consideration is taken when adding Fe. The above research gaps have motivated the study to design metastable β alloy with high Mo and low Fe as a low-cost alloying elements. The aim of the study is to stabilize the β phase with minimal formation of α″+ω phases, thus resulting in elastic modulus much lower than that of Ti-6Al-4 V alloy and moderate strength. The objective of the study is to explore how different values of electronic parameters such as Molybdenum equivalence (*Moeq*), electron to atom ratio (*e/a*), and the *Bo* and *Md* phase stability map influences the phase stability, and also understand how the resulting β phase stability affects mechanical properties when small addition of Fe is added to Ti-17Mo in attempt to further increase the strength of the alloy. Thus, the two alloys that are currently investigated are binary Ti-17Mo and ternary Ti-16.5Mo-1.1Fe alloys.

Table 1 Designated name, composition, the calculated *Moeq*, *e/a* ratio and average *Bo-Md*

Designated Alloy Name	Alloy Composition (wt%)	Moeq (wt%)	e/a ratio	Average Bo	Average Md
Alloy A	Ti-17Mo	17.0	4.19	2.82	2.40
Alloy B	Ti-16.5Mo-1.1Fe	19.7	4.22	2.81	2.39

Materials and methods

Molybdenum equivalence (*Moeq*)

The molybdenum equivalence (*Moeq*) is an expression that represents the contribution of each alloying element towards β phase stability when they are compared to the most effective β stabilizer which is Molybdenum (Mo). Molybdenum equivalence concept was first proposed by Molchanova et al. (Molchanova and Glazunov 1965) and it was later modified by Bania in 1994. The modified coefficient of each β-stabilizers was calculated as the ratio of critical minimum level of β stabilizing content of Mo which reported by Bania to be 10 wt% (Bania 1994). Thus, the stability of β phase in Ti alloys which is dependent on theory in other words, the weight% (wt%) of the alloying elements necessary to suppress martensitic transformation temperature (Ms) in the β-Ti alloy can be predicted by quantitative rule of *Moeq*. The calculated *Moeq* values of the two currently considered alloys are illustrated in Table 1, indicating that *Moeq* values where they show that Alloy 1 and Alloy 2 are higher than 10 wt% in both alloys, suggesting that both alloys will stabilize the β phase when quenched from high temperatures.

Theoretical d -method alloy design

A molecular orbital method was employed where electronic structures were calculated for body centered cubic (bcc) Ti alloyed with a variety of alloying elements (Morinaga 2016; Kuroda et al. 1998). Two alloying parameters were determined theoretically, one is the bond order (hereafter referred to as *Bo*) which is a measure of the covalent bond strength between Ti and an alloying element. The other is the metal d-orbital energy level (*Md*) which correlates with the electronegativity and the metallic radius of elements (Abdel-Hady et al. 2006). The average values of *Bo* and *Md* are defined by taking the compositional averages of the parameters respectively (Li et al. 2013a, b; Ahmed et al. 2015). The average *Bo* and *Md* and their composition are presented in Table 1. Figure 1 is a phase stability map (called the *Bo-Md* map) in which the areas of α, α + β and β type alloys are separated clearly. The position of Ti alloys are shown by symbols such as a circle and diamond shapes in Fig.

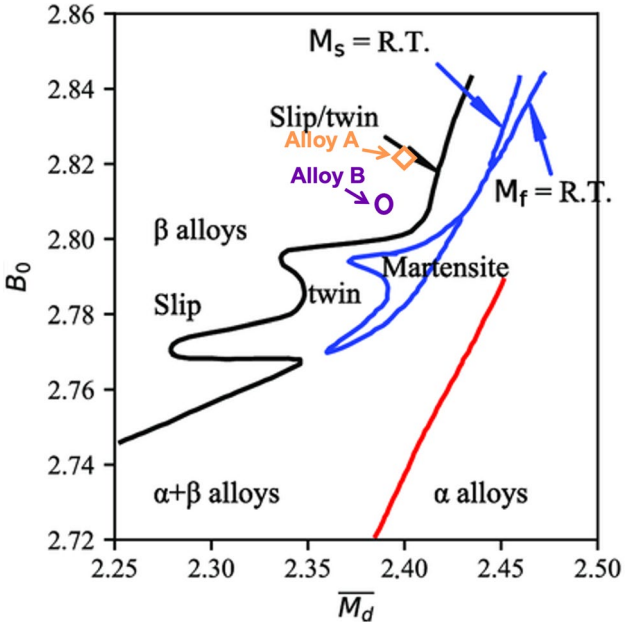

Fig. 1 Phase stability diagram based on the average *Bo* and *Md* parameters (Morinaga 2016; Kuroda et al. 1998; Abdel-Hady et al. 2006; Morinaga et al. 1986)

1. The values of moduli of elasticity for these alloys are decreasing with increasing average *Bo* and *Md* values in β type alloys regions on the phase stability (Kuroda et al. 1998). According to the phase stability map in Fig. 1, both Alloy A and B are both within the β region, this implies that both alloys will stabilize the β phase, while upon quenching from high temperature. The calculated *Bo* and *Md* values presented in Table 1 demonstrates that when 1.1wt.% of Fe is added as third alloying element both the *Bo* and *Md* values decrease slightly, this could be affected by the addition of Fe which has a smaller atomic radius and electronegativity as compared to Mo and Ti. The decrease in *Bo* and *Md* values might indicate that the elastic modulus might increase as the results contradict the statement made by Kuroda et al., that states that when *Bo* increases and *Md* decreases the elastic modulus will decrease (Kuroda et al. 1998).

The electron-to-atom (*e/a*) ratio method

Another theoretical prediction mostly used in research studies is the electron to atom (*e/a*) ratio which is used to predict the average number of valence electron for each atom (Ikehata et al. 2004). The Hume-Rothery showed that the *e/a* ratio of metals and alloys is vital in controlling the phase stability and phase transition boundaries, where *e* and *a* represent the number of free valence electrons for each atom (Hume-Rothery et al. 1934). According to Tiwari et al.,, the phase stability of metals and alloys are determined by free energy that can be attributed to the change in electronic energy or the misfit or strain energy (Tiwari and Ramanujan 2001). Previous works (Wang et al. 2017); Buzatu et al. 2016) have indicated that the phase stability of Ti alloys is related to the *e/a* ratio. The function of *e/a* ratio and the expected phase constituents after water quenching are depicted in Fig. 2 (a) where the stability of the β phase in Ti alloys increases with the *e/a* ratio and the stability limit of a Ti alloy with a fully β phase was reported to be around 4.20 and below this value presence of other phases such as ω and α″ can occur (Laheurte et al. 2010).

The elastic modulus of metastable β Ti alloys is related to phase constituents as indicated in most literature work (Zhou and Niinomi 2009). Figure 2 (b) illustrate a relationship between the elastic modulus, phase constituents and the *e/a* ratio. It can be seen from the diagram that low modulus is seen when the *e/a* ratio is between 4.07 and 4.09, beyond these values (4.1–4.19) the elastic modulus increase significantly and below these values

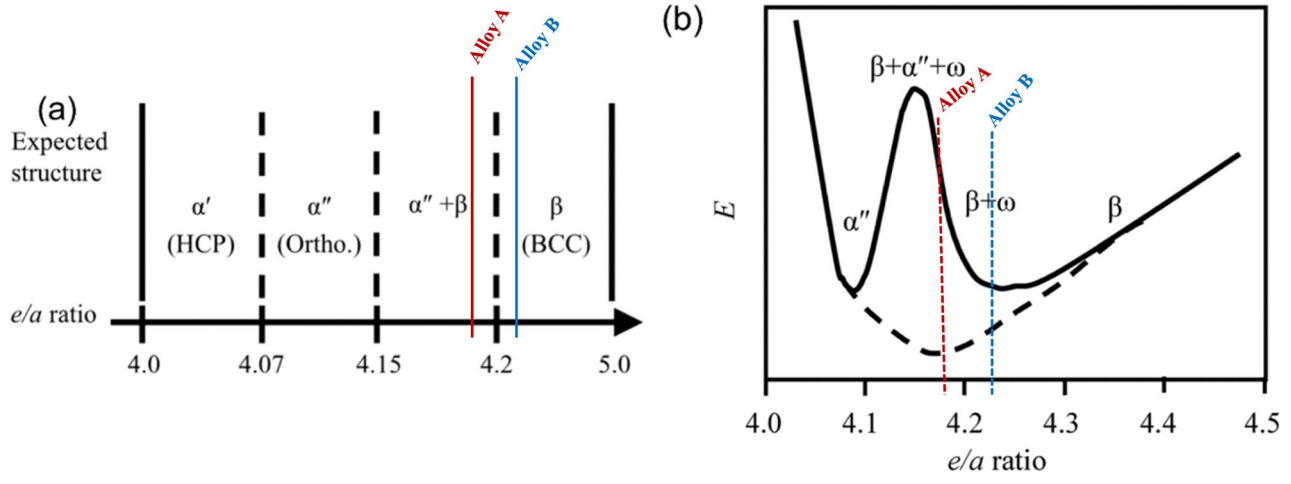

Fig. 2 Expected phase constituents in the microstructure of Ti alloys after quenching from high temperature versus e/a ratio, reproduced from Refs (Liang 2020; Laheurte et al. 2010). **a** and the relationship between elastic modulus with e/a ratio in Ti alloy systems (Zhao et al. 2022) **b**

the modulus start to decrease slightly. Several researchers have designed new Ti alloys with low elastic modulus using the *e/a* method and they reported on the relationship between *e/a* ratio and the phase boundary and the effect of phase constitution on the elastic modulus (Lee et al. 2012). Table 1 present the *e/a* ratio of the designed alloys where Alloy A illustrate an *e/a* ratio of 4.186 and Alloy B with 1.1 wt% Fe shows an *e/a* ratio of 4.139. The calculated *e/a* ratio and the *e/a* ratio demonstrated in the diagrams demonstrate that Alloy A will exhibit β + α″, while Alloy B will possess β phases upon quenching from high temperature and also indicate that Alloy A will show high elastic modulus because of the presence of both β, α″ and high ω phase and Alloy B is predicted to exhibit low elastic modulus because of low content of ω phase and the presence of β phase.

Materials preparations and fabrication process

Two metastable β-type Ti-Mo alloys, namely, binary alloy containing 17 wt% Mo and a ternary alloy of Ti-16.5Mo-1.1Fe wt% composition (referred to as Alloy A and Alloy B, respectively) were investigated in this study. High purity metallic powders were weighed according to targeted composition and cold compacted into green bodies using the Zwick-Roell testing machine with a maximum load of 80 kN and cross head speed for 20 mm/min. The compacted green bodies were melted using the AMAZEMET rePowder Plasma melting system which operates under high inert environment (Żrodowski et al. 2021). The system was purged with argon to minimise the oxygen content in the chamber to at least to less than 100 ppm and pure titanium was melted to act as oxygen-getter. This process use an arc with current starting from 70 A to 270 A to melt the powder compacts. Without opening the chamber, the ingot is turned and re-melted 4 times on the water cooled copper hearth to attain better homogeneity. The ingots were solution treated in a muffle furnace at 1100 °C, held for an hour and quenched in ice-brine, thereby referred as water quenched (WQ) samples.

Phase and microstructural characterization

Phase analysis was executed using X-ray diffractometer (Malvern Panalytical Empyrean Diffractometer). XRD patterns were run with Cu Kα radiation with a secondary monochromatic (λ = 0.1545 nm) at 45 kV and 40 mA. The 2θ scan range is from 5° to 100 ° at a step size of 0.01°. A reference silicon disk is run at the same conditions as verification. X-Pert High score was used to detect the phase constituent of as-cast Ti-Mo-Fe alloys. Optical microscope (OM) specimens were prepared following the metallographic preparation techniques and they were etched using Kroll etchant (90 ml H_2O, 2 ml HF, 3 ml HNO_3 and 5 ml HCl.) for 30–60 s. The OM micrographs were analysed using the Leica optical microscope (Olympus DSX-HRSU. SN: 5H42695, Tokyo, Japan). The elemental analysis on heat-treated samples were conducted using energy dispersive X-ray spectroscopy (EDS) embedded within the JOEL JSM-6010 Plus/LAM scanning electron microscope (SEM) operating at an accelerating voltage of 8 kV. In order to obtain clear images within large grains, the images were taken at higher magnifications.

To further investigate the phase analysis or present of phases, electron backscatter diffraction (EBSD) technique was used. EBSD samples were prepared by electropolishing them using a Struers electro-polishing machine at 30 V for 80s. The EBSD scans of all the samples were were performed using Zeiss Cross Beam 540 equipment operating at 25 kV and 10 nA to image the samples. The EBSD analysis were performed using an Oxford NordLys Max detector and Oxford Aztec analysis software. Band contrast images and phase maps were constructed. The grain size measurements on the micrographs were conducted using Image J software.

Tensile and hardness properties

Micro-Vickers hardness for all the water-quenched samples was measured using the Zwick Roell Vickers hardness indenter. The indents were made from a small diamond under the load of 500gf for 10s. For each sample, 10 indents were made with a 2 mm distance and measured microscopically and finally, their averages were recorded. Tensile specimens of 40 × 5 × 3 mm were prepared by electrical discharge machining. Tensile tests were performed at room temperature using an Instron™ 1342 tensile tester fitted with 50 kN load cells with a constant crosshead speed of 0.5 mm/min. An extensometer was attached to the gauge section of the test specimen and was used to measure the tensile strain. The fracture surfaces of the tensile specimens were analysed using JOEL JSM-6010 Plus/LAM scanning electron microscope (SEM) at accelerating voltage of 8 kV and all the images were captured at a magnification of 350 (50 µm scale bar).

Results and discussions

X-ray diffraction

X-ray diffractometer (XRD) technique was used to detect phases present in Alloy A and Alloy B. The corresponding XRD patterns are depicted in Fig. 3 (a and b). XRD patterns of both alloys after quenching from high temperature indicated peaks belonging to only β phase. It is interesting to note that the most intense peak in both metastable βTi alloys is at 2θ = 85° along (220) crystal plane, reflecting the abundance of atoms in this plane, as opposed to typical 2θ = 40° along (110) plane for stable BCC crystals. This change in highest peak intensity could be linked to strong possibility of omega (ω) phase presence, with Alloy A displaying the highest ω phase

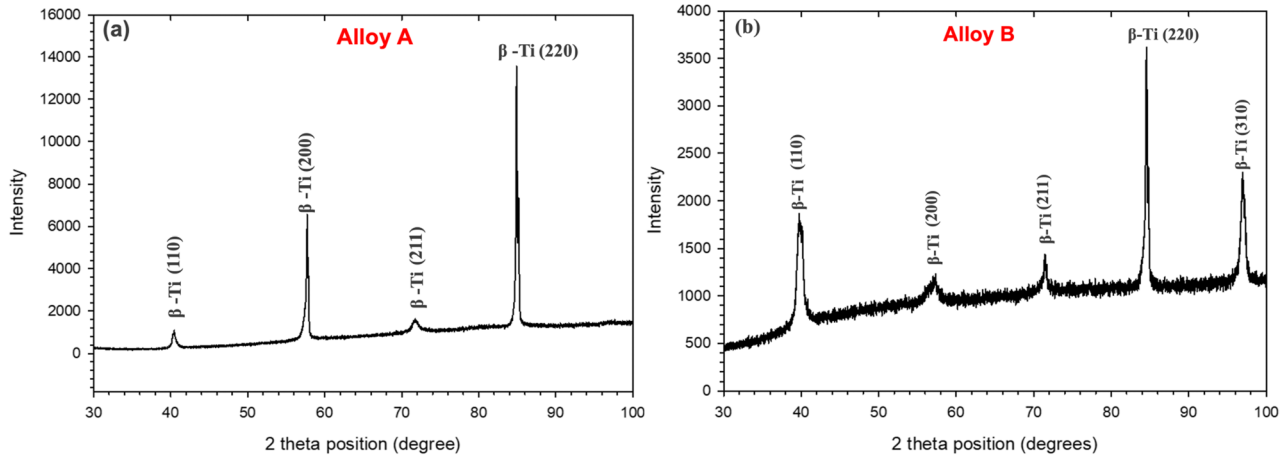

Fig. 3 X-ray diffraction patterns of (**a**) Alloy A and (**b**) Alloy B upon water quenching

presence signalled by highest atomic density along (220) crystal plane. On the other hand, the peak width in both alloys were generally narrow, an indication of higher crystallinity, with little difference. The predictions by *e/a* ratio in both alloys indicated that both alloys are likely to possess the orthorhombic martensitic phase (α″) and athermal omega (ω) phase after quenching from high temperatures. However, both phases were not detected in both Alloy A and Alloy B using the XRD technique because of the following: the absence of martensitic phase could indicate that the martensitic start transformation (*Ms*) temperature is below room temperature for both alloys. It is well known that the martensitic start transformation (*Ms*) temperature of β-isomorphous alloys decreases as the solute content increases (Davis and Flower 1979; Hanada and Izumi 1986). This view is in agreement with the previous studies by (Zhou and Luo 2011; Bagariatskii et al. 1958). The existence of XRD peaks belonging to α″ phase is widely reported in literature in alloys with lower content of Mo such as Ti-12Mo, Ti-10Mo, Ti-15Mo alloys (Ho et al. 1999; Moshokoa et al. 2024; Raganya et al. 2021), thus it was evident from the current study that in binary Ti-Mo alloys with higher Mo content, the orthorhombic martensite phase was not observed. The other phase such as the hexagonal athermal omega (ω) phase was not distinguished in the XRD patterns and this could be a result of it's low detection limit when using this technique. Earlier investigations by Zhao et al. and Sabeena et al. pointed out the presence of the precipitation of the athermal omega (ω) phase from Ti-10Mo to Ti-20Mo alloys (Zhao et al. 2012a, b; Sabeena et al. 2017). However, according to Sun et al., and Nakai et al. the ω phase is difficult to detect by XRD since β and ω phase peaks overlap (Sun et al. 2013; Nakai et al. 2011). Therefore, the presence of the α″ and ω might be revealed by using high characterization techniques such as TEM (Transmission Electron Microscope) and EBSD (Electron Backscatter Diffraction).

The XRD patterns in TM17 alloy are in agreement with those reported by Zhou et al. (Zhou and Luo 2011), where a fully β phase peaks in Ti-17Mo alloy after quenching was reported. Ternary alloys such as Ti-2Mo-xFe and Ti-3Mo-xFe (x = 0.5, 1.0, 1.5 and 2.0 at%) were investigated by Kobayashi et al. and were not comparable to current XRD peaks belonging to Alloy B, as those showed presence of the orthorhombic martensitic phase (α″) and hexagonal athermal omega (ω) (Kobayashi et al. 2014),. Abd elrhman et al. reported the presence of peaks of orthorhombic martensitic phase (α″) and bcc β phase in Ti-4.7Mo-4.5Fe at% (Ti-9Mo-5Fe wt%) (Abd-elrhman et al. 2016). The XRD technique showed that the designed alloys, binary alloy with high Mo and a ternary alloy with the addition of 1.1 Fe wt%, have the ability to stabilize the β phase when quenched from above the β-transus temperature without forming other phases when characterized using the XRD technique. The phases predicted by the predictive tools such as *e/a* ratio in Alloy A in Fig. 2 (a) were not in accordance with the experimental XRD results, however the *Moeq* and *Bo-Md* predicted results were in agreement with experimental data.

Optical microscope

Optical microscope (OM) technique was employed to analyse the microstructural features of both alloys after quenching. Figure 4 represents the optical micrographs of Alloy A and Alloy B respectively. As shown in Fig. 4 (a), Alloy A depicts a micrograph composed of very large grains of β-equiaxed grain and with fine substructures precipitated inside the grains and along the grain boundaries. The fine substructures could be associated with either orthorhombic martensitic structure or athermal omega structure. Thus, highly sensitive characterization techniques are required to confirm the crystal

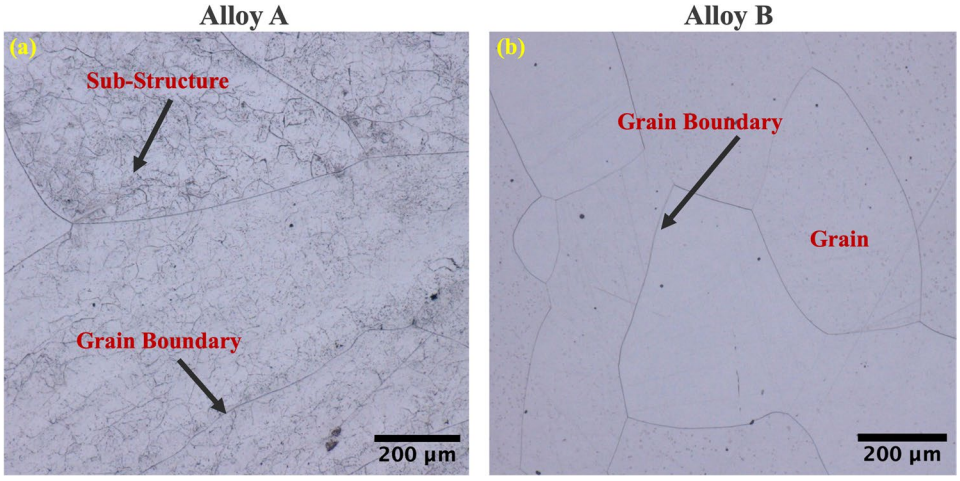

Fig. 4 Optical microscope (OM) micrographs of water quenched (**a**) Alloy A and (**b**) Alloy B

structure of the observed substructures as they could not be detected by XRD technique. Depending on the stability of the β structure which depends on the composition, and cooling rate, other phases may precipitate upon quenching. It is reported that crystal structure of martensite phase formed in alloys with low β solute content changes from hexagonal (α') to orthorhombic (α″) with increasing the β solute content (Li et al. 2019; Kolli and Devaraj 2018). Due to the possible impact of these phases/structures on the mechanical properties of Ti alloys, the prediction of their formation is of great interest. The *e/a* ratio and the phase stability map predicted that Alloy A will possess orthorhombic martensitic structure and the hexagonal athermal omega after quenching. Since the fine substructures could not be quantified by XRD, they could be associated as either belonging to hexagonal athermal omega structure or orthorhombic martensitic structure. Moreover, the precipitation of substructure was in agreement with the results illustrated by the predictive tools.

Optical micrograph of Alloy B in Fig. 4 (b) possessed only β equiaxed grains without any presence of substructures and the grains were observed to be smaller as compared to Alloy A. The experimental results of Alloy B are not in agreement with the *e/a* ratio phase prediction, however they agreed with the predictions by the *Moeq*, *Bo* and *Md* phase stability map in Fig. 1. The OM micrographs were in agreement with the XRD peaks presented in Fig. 3 whereas OM micrograph of Alloy A was not completely in agreement with the corresponding XRD results in Fig. 3.

Energy dispersive spectroscopy (EDS)

To determine the elemental analysis of the two alloys after processing, SEM equipped with EDS capability was used. Figure 5 represents the EDS analysis of Alloy A and Alloy B respectively, where point and shoot were done at different place. The results in Alloy A showed that the area within the grains where there are no substructures depicted Mo-rich areas as compared to the the area on the grain boundaries composed of substructures. The results in Alloy B illustrated that area 2 which was by the grain boundaries was Mo-rich but lean in Fe whereas the areas within the grains were little bit high in Mo and low in Fe, although area 2 was rich in Mo as compared to area 1. According to the EDS results, very minimal segregation did occur in Alloy A and Alloy B. The concept of segregation is common in metastable β Ti alloys, for instance Ruzic et al. reported on effect of Mo segregation in Ti-12Mo alloys which were investigated using nanoindentation methods (Ruzic et al. 2018).

EBSD band contrast and phase maps

The EBSD band contrast of the two alloys were analysed to illustrate the grains in each alloy better as opposed to the ones in the OM micrographs and the EBSD contrast were analysed to further show if the alloys were composed of other structure other than the ones that were present when examining using the OM. The EBSD contrast and IPF maps are presented in Fig. 6 (a & b) and (d & e) respectively. The EBSD contrast in Alloy A, showed no substructures or any other phases that were noticeable in the OM micrographs but the β equiaxed grains with coarser grains (grain size of 393 µm) were more visible. The absence substructures in the EBSD contrast could be due to segregation that is reported to occur in metastable β-Ti alloys during melting and casting and that was noticeable in the EDS results (Ruzic et al. 2018). The area that was analysed in the EBSD might not be same as the one position that was analysed in the optical microscope. The EBSD contrast in Alloy B showed significantly finer β equiaxed grains with a grain size of 146 µm without the presence of any other structures. The EBSD phase maps, Fig. 6 (c and f) respectively were evaluated to determine

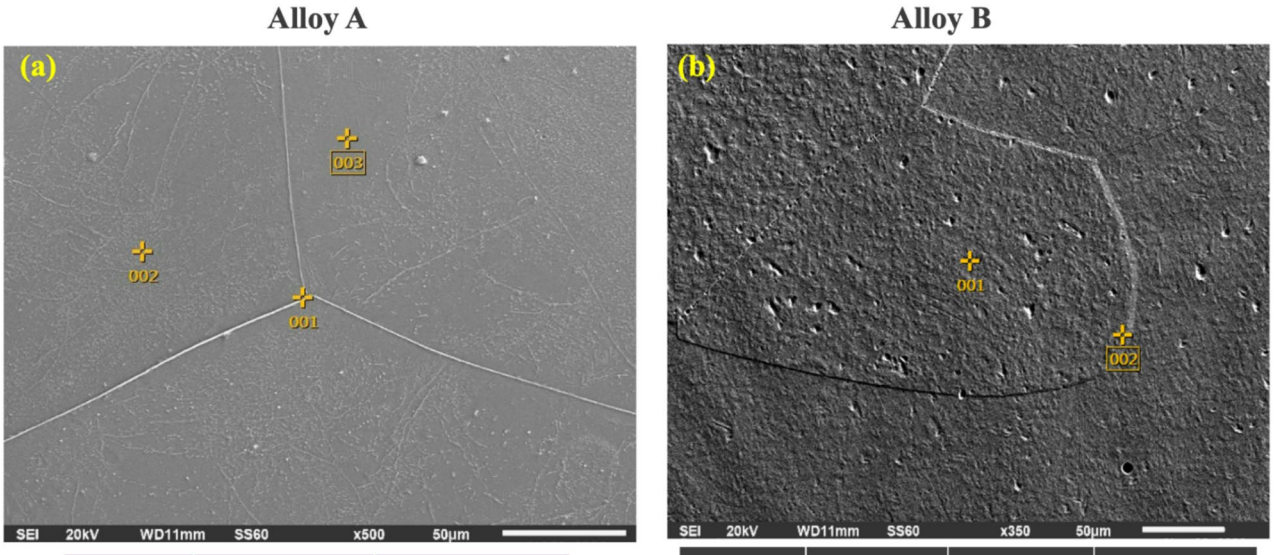

	Ti (wt%)	Mo (wt%)
1	82.90	17.10
2	82.28	17.72
3	82.00	18.00
Average	**82.39**	**17.61**

	Ti (wt.%)	Mo (wt.%)	Fe (wt.%)
1	82.20	16.81	1.00
2	80.74	18.44	0.82
Average	**81.47**	**17.63**	**0.91**

Fig. 5 EDS analysis of water quenched (**a**) Alloy A and (**b**) Alloy B

the presence of other phases that were not detected using the XRD technique. Both Alloy A and Alloy B showed the presence of ω and β phase, in addition to these phases Alloy A depicted low volume fraction of the existence of α″ phase. The volume fraction of ω in Alloy A was higher as compared to Alloy B, the results indicated that the ω phase do existence in metastable Ti alloys with higher Mo concentration and this phase have the ability to affect the mechanical properties: strength and elastic modulus.

Tensile properties

Ultimate tensile strength

The design of an orthopedic implant must meet certain requirements such as mechanical compatibility, biocompatibility, because a human bone is a dynamic tissue which is continuously being remodelled to adopt variable mechanical loads (Abdel-Hady Gepreel and Niinomi 2013). Remodelling bone tissue entails replacing old bone tissue with new bone (Arias et al. 2018). Thus an implant must possess acceptable mechanical properties such as strength to endure loads and resist fracture (Asri et al. 2017). Other essential mechanical properties that decide the type of a material are hardness, elongation, elastic modulus and fatigue strength. To investigate the mechanical properties of the designed alloys, tensile strength was performed at room temperature on three specimen per alloy and their mechanical properties were recorded. Figure 7 illustrate the ultimate tensile strength (UTS) of Alloy A and Alloy B. It was observed that when Fe was added as a third element, the tensile properties (UTS and E) decreased significantly. Alloy A displayed a tensile strength of 912 MPa, whereas the tensile strength of Alloy B was found to be 540 MPa. There are several factors that affect the strength of a material, this includes the phase constituents, the microstructure which include the solid solution strengthening, dispersion hardening, deformation mechanism and grain size, etc. The presence of phases influences the strength of a material in the following manner according to Lee et al.: $S_{\omega} > S_{\alpha'} > S_{\alpha''} > S_{\beta} > S_{\alpha}$ (Lee et al. 2002). From the above factors, it is most likely that the high strength in Alloy A is as a result of solid solution strengthening whereas the lower strength in Alloy B is attributed to strong β phase stability and hardening driven by presence of Fe with smaller atomic radius than both Ti and Mo. As revealed by EBSD phase maps in Fig. 6 (c), Alloy A showed high volume fraction of the athermal omega (ω) phase and presence of orthorhombic (α″) martensitic phase, alongside the β phase as opposed to Alloy B which is mainly comprised of β phase and reduced amount of ω phase. The other reason for the difference in strength could be attributed by presence of the fine sub-structures that are associated with very fine

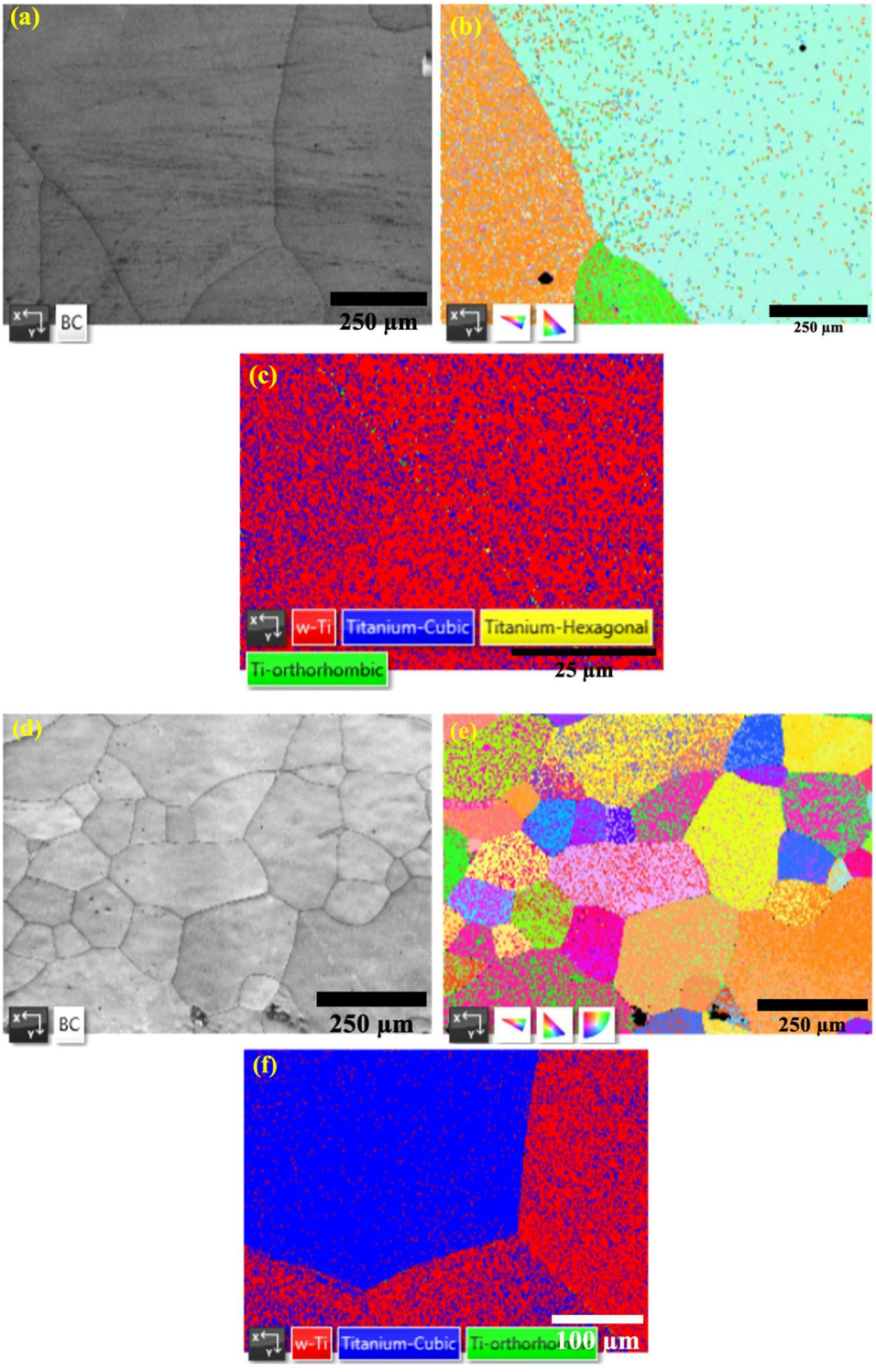

Fig. 6 EBSD band contrast, IPF maps and phase maps of water quenched Alloy A (**a**-**c**) and Alloy B (**d**-**f**), respectively

athermal omega or orthorhombic structure as observed in the OM micrographs. Moreover, the ω phase is known to be a harder phase than the α″ or β phase, and thus a high density of the fine ω particles will strengthen the alloy more (Lin et al. 2002).

The UTS of Alloy A was notably higher as opposed to other binary alloys that were explored in literature such as Ti-17Mo with a UTS of 750 MPa, higher than the UTS of 700 MPa and 800 MPa in Ti-16Mo and Ti-18Mo alloys, respectively, which were investigated by Zhao

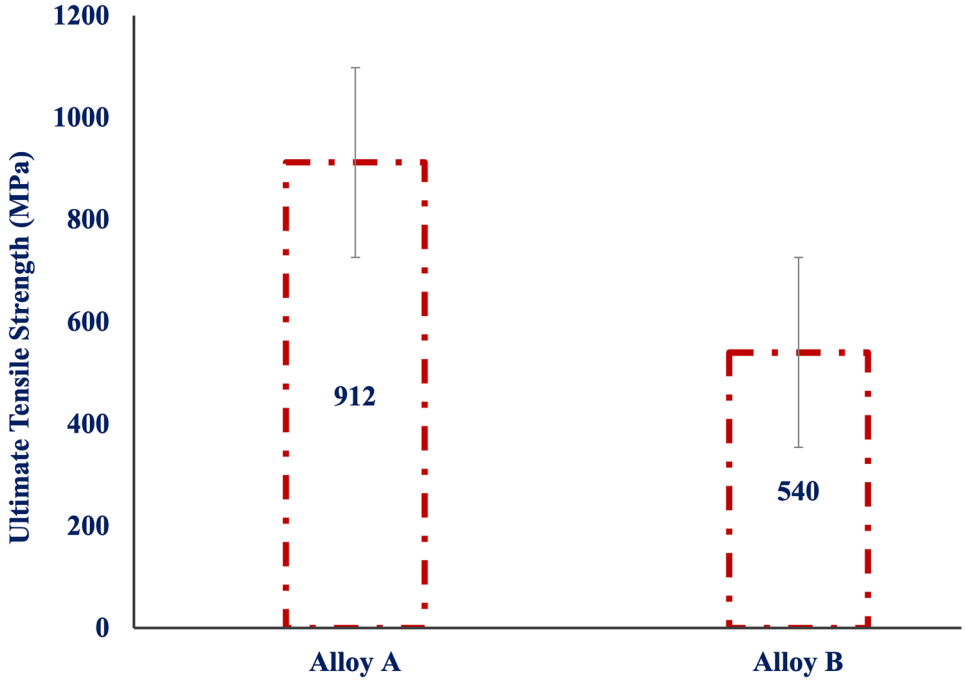

Fig. 7 Ultimate tensile strength of Alloy A and Alloy B

et al. (Zhao et al. 2012a, b). On the other hand, due to higher Mo content which resulted in β single phase and less work reported on the tensile properties of Alloy B, the UTS of Alloy B were compared with other Ti-Mo-Fe alloys that are reported in literature. The UTS of Alloy B was found to be significantly lower as opposed to the UTS of Ti-2Mo-0.5Fe at% (949 MPa) and Ti-3Mo-0.5Fe at% (800 MPa) that were subjected to different processing which were studied by Abdel-Hady Gepreel et al. (Abdel-Hady Gepreel and Niinomi 2013; Abd-elrhman et al. 2016) and the UTS of Alloy B was found to be notably lower that UTS of Ti-9Mo-5Fe (975 MPa) which underwent different processing and was reported by Abd-elrhman et al. (Abdelrhman et al. 2019a, b). The UTS of Alloy B was found to lower as found to be lower in comparison to the annealed UTS of Ti6Al4V alloy (825–892 MPa), however the UTS of Alloy A was higher than that of commercially available Ti6Al4V alloy. The high strength in Alloy B shows potential to be considered for biomedical applications such as orthopedic implants and those of vascular stents, but Alloy B can be further be processed to improve its tensile strength because the alloy depicted no intermetallic phases or dendrites that will contribute to its brittleness.

Elastic modulus

Elastic modulus is the resistance offered by the material against deformation when the load is applied, and it must not exceed that of the cortical bone because it will result to what is called a stress shielding effects which is not desirable as it leds to implant failure (Zhang and Chen 2019). Figure 8 demonstrate the elastic modulus of the studied alloys, where Alloy A depicted an elastic modulus of 82 GPa and Alloy B with low elastic modulus of 74 GPa. According to literature, elastic modulus can be affected by factors such as microstructural constituents, solid solution phenomenon, presence of phases, processing techniques ect. According to Hao et al. (Hao et al. 2002), elastic modulus of different phases of Ti-alloys decrease in the following way: $E_{\omega} > E_{\alpha} > E_{\alpha'} > E_{\alpha''} > E_{\beta}$. The trend shows that an alloy that possess the presence of ω phase will exhibit high elastic modulus as opposed to the alloy with β phase. It is well reported in literature that the ω phase has a significant effect on the mechanical properties of Ti alloys and it is likely to increase the elastic modulus (Akahori et al. 2005). Thus, the high elastic modulus in Alloy A might have been attributed by the high volume fraction of ω phase and existence of α″ phase that were observed in the EBSD maps in Fig. 6 (c) and the high elastic modulus might be due to the presence of substructures that were seen in the OM micrographs in Alloy A. The low elastic modulus in Alloy B might be due to the low presence of ω phase as seen in the EBSD maps in Fig. 6 (f) and the presence of only β equiaxed grains as indicated in the OM micrographs.

The elastic modulus in Alloy A agrees with the results predicted by the *e/a* ratio in Fig. 2 (b), as it predicted that an alloy within that *e/a* range of 4.1–4.2 will likely to possess high modulus as compared to an alloy with an *e/a* ratio that is more than 4.2. The low elastic modulus

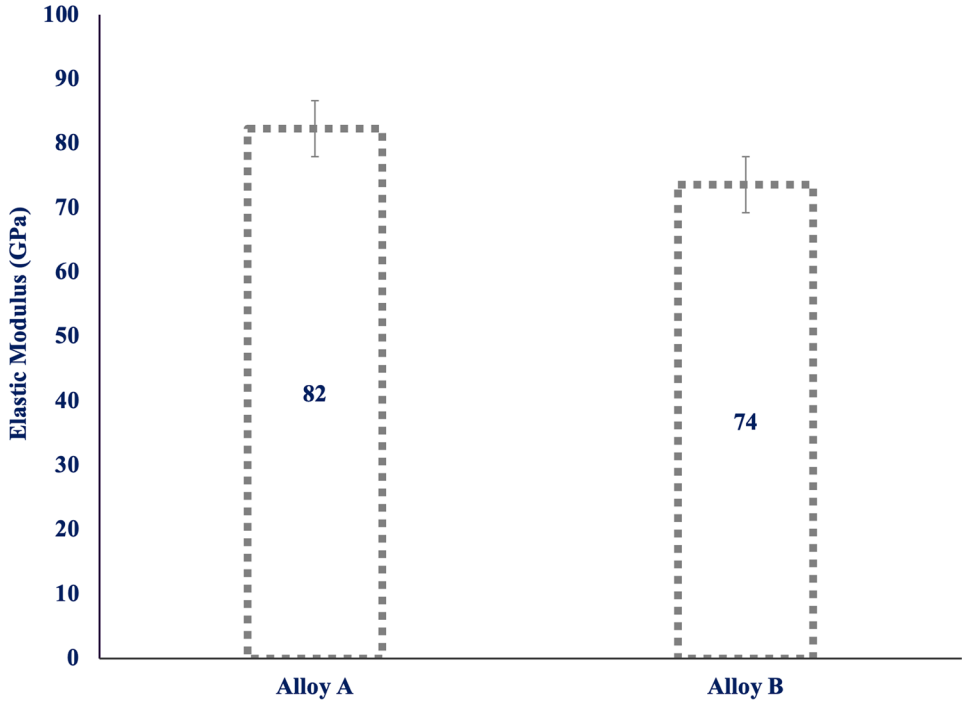

Fig. 8 Elastic modulus of Alloy A and Alloy B

in Alloy B could be due to its high *Moeq* value that predicted β stability that lead to low elastic modulus. Comparing the studied alloy with those available in literature, it was seen that the elastic modulus in Alloy A was notably higher as compared to the elastic modulus of 73 GPa, 78 GPa, and 75 GPa in Ti-17Mo, Ti-16Mo and Ti-18Mo alloys respectively that were studied by Zhao et al. (Zhao et al. 2012a, b).,. Due to current limited studies on Ti-Mo-Fe alloys with higher Mo composition, the elastic modulus in Alloy B was compared to published Ti-Mo-Fe alloys with low composition of Mo such as Ti-2Mo-0.5Fe (84 GPa), Ti-2Mo-1.5Fe at% (117 GPa), Ti-3Mo-0.5Fe at% (81 GPa) and Ti-3Mo-1.5Fe at% (119 GPa) which were investigated by Kobayashi et al. (Kobayashi et al. 2014; Ion et al. 2021; Song et al. 1999)They were also compared to the elastic modulus reported by Abdel-Hady Gepreel et al.(Abdel-Hady Gepreel and Niinomi 2013; Abd-elrhman et al. 2016) in Ti-4Mo-1Fe (85 GPa) and Ti-6Mo-1Fe (82 GPa). The elastic modulus of both alloys were significantly lower as compared to the commercially available Ti6Al4V alloy. Alloy B showed better potential as a candidate alloy that can considered to be used as a biomaterial for orthopedic implants because of its ability to stabilize the β phase with only solution treatment process and possesses lower elastic modulus. However, Alloy A with high elastic modulus and higher strength, which can still be improved further by other thermomechanical processes, shows potential to be considered for other biomedical applications such as vascular stents (Gordin et al. 2020; Ion et al. 2021).

The mechanically compatible performance of a material intended for biomedical application and it can be evaluated by the elastic admissible strain (EAS) (Song et al. 1999).The elastic admissible strain is defined as the ratio of yield strength or tensile strength to elastic modulus (Abdel-Hady Gepreel and Niinomi 2013). It is a useful parameter for the design of orthopedic implant and it should be exploited in order to prevent failures due to fatigue and the onset of stress-shielding effect which is associated with high elastic modulus (Dal et al. 2018). The higher the elastic admissible strain, the more desirable the material is for biomedical applications. The EAS of Alloy A was higher and that of Alloy B was lower. The results indicate that for the EAS to be higher it must possess high strength and low elastic modulus to meet the requirement for orthopedic implants. High elastic modulus contributed to high EAS, thus rendering Alloy A desirable for biomedical application such as vascular stent applications as opposed to orthopedic implants.

Micro-Vickers hardness

Micro-Vickers hardness results of Alloy A and Alloy B are presented in Fig. 9. Hardness increased notably with the addition of Fe content, the hardness increased from 366 $Hv_{0.5}$ in Alloy A to 428 $Hv_{0.5}$ in Alloy B. According to published work, hardness of a material can be attributed by several factors such as the grain size, the microstructure or phase present, the processing technique and the cooling medium (Jamhari et al.

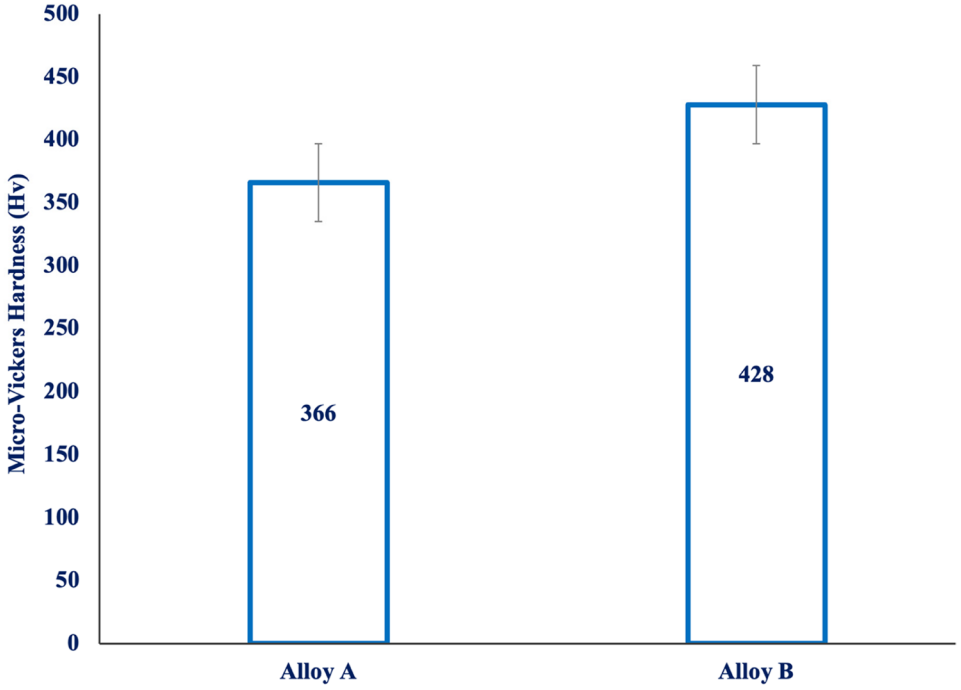

Fig. 9 Micro-Vickers hardness of Alloy A and Alloy B

2023). In addition, Furukawa et al. stated that hardness has a connection with the structure of a material, for example, it has a connection with the grain size, the distance between the particles of the intermediate phases (Furukawa et al. 1996; Hall 1951). As per the Hall-Petch mechanism the grain boundaries acts as a barrier to the dislocation movement. Smaller grains makes it difficult for dislocations to move and this results in an increase in the hardness, whereas big grains allows free movement of dislocations and therefore decrease the hardness of a material. Although it is reported that reducing grain size can simultaneously increase the strength and ductility in the metastable titanium alloys (Bhattacharjee et al. 2006), the above explanation provided clarity on the hardness difference between Alloy A and Alloy B. According to the optical micrographs in Fig. 4(a), Alloy A depicted bigger grains as compared to smaller grains of Alloy B in Fig. 4 (b), the EBSD band contrast in figure also depicted coarser grain with a grain size of 393 μm in Alloy A and finer grains with grain size of 146 μm in Alloy B. The bigger grains in Alloy A led to low hardness as dislocations were able to move freely without restrictions, whereas Alloy B with smaller grains restricted the movement of dislocations which led to dislocation pile up and strengthening of a material. The hardness of both alloys were notably higher as compared to Ti6Al4V (288 Hv) alloy reported by Guo et al. (Guo et al. 2022). The hardness in Alloy B was higher as compared to Ti-2.0Mo-0.5 at.%Fe (327 Hv), Ti-3Mo-0.5Fe at% (270 Hv) and Ti-3Mo-1.5Fe at% (401 Hv) presented by Kobayashi et al.(Kobayashi et al. 2014).

Fracture surfaces

The micrographs of fracture surface after tensile test at room temperature along different orientation is depicted in Fig. 10 (a) and (b). As illustrated, the micrographs in both alloys are characterized by the presence of tearing bridges, cracks along the grain boundaries, cleavage facets signifying brittle fracture. There were thin parallel lines visible that could not be distinguished if whether they belong to the orthorhombic martensitic structure. The appearance of coarse particle boundary facets indicated an enhanced embrittlement trend of the alloy, which ultimately leads to poor ductility due to the intergranular fracture (Rao et al. 2006). The fracture surface of both alloys were composed of large β equiaxed grain with intergranular cleavage facets, coarse dimples with less tearing ridges and microvoid coalescence. The results implied that the Alloy B exhibited a combination of brittle and ductile fracture.

Biocompatibility and long performance of metastable beta Ti alloys

Biocompatibility in Ti alloys for biomedical applications stems from its inertness, strength to weight ratio, flexibility with mirroring the bone, non-toxic elements, lack of immunogenicity ect, hence it is vital to characterize the biocompatibility of new composition and the effect of processing (Bahl et al. 2021).

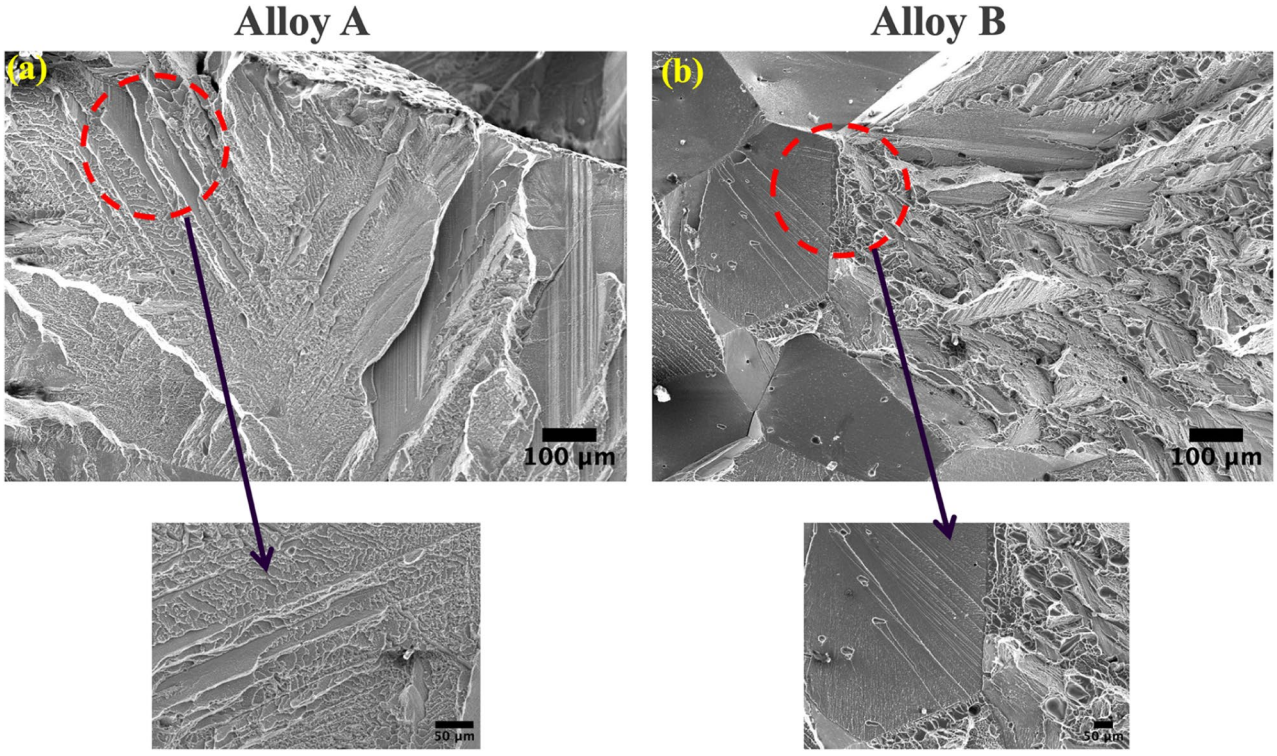

Fig. 10 Fractography of (**a**) Alloy A and (**b**)) Alloy B

Biocompatibility can be tested in corrosion and wear properties because the two affect the life span of alloys. Currently, corrosion and wear behaviors of Ti-Mo alloys are usually studied separately as isolated systems (Oliveira and Guastaldi 2009). But implants are generally encompassed by body fluids in the human body that induces corrosion. Also, there is relative motion between the implant and bone as well, such as sliding and fretting. Therefore, wear and corrosion can occur simultaneously when the alloys are implanted into the human body. Biocompatibility can also be tested in vitro and in vivo test (Bahl et al. 2021). In vitro tests evaluate attachment, proliferation, and differentiation of osteoblasts or stem cells. Viability of fibroblasts often serves as a measure of cytotoxicity of alloys. To ascertain Ti's safety and effectiveness, it is often subjected to in-vitro cytotoxicity evaluations using specific cell types like L929 and MC3T3 E1 cells. Through these tests, Ti's viability and reliability as an implant material are consistently demonstrated. Various studies have demonstrated the investigation of cell culture and response in metastable β-Ti alloys, for instance a study by Abdelrhman et al. evaluated the biocompatibility of new low cost Ti-Mo-Fe alloy using cytotoxicity test which was carried in a murine-derived MC3T3-E1 cell line, where the results high cytocompatibility between Ti-Mo-Fe alloys which was higher than Ti6Al4V alloy (Abdelrhman et al. 2019a, b),. Another study by Mostafa et al. evaluated the in vitro and in vivo test in Ti-4.7Mo-4.5Fe and Ti-3Mo-0.5Fe alloys by using cytotoxicity test which was conducted in murine derived MCT3T3-E1 cell line for in vitro test and for in vivo, the test was done in six male V Spain while rabbits who were 6 months. The results showed that Ti-3Mo-0.5Fe alloy showed significant potential for bioactive osteogenic activity and excellent biocompatibility (Mostafa et al. 2025),. The literature studies show much potential for Ti-Mo-Fe based alloys to be biocompatible alloy to be considered for biomedical applications. The current study did not evaluate the corrosion resistance or cytotoxicity test of the studied composition, however the above literature pave ways for the biocompatibility test of the investigated composition to further be evaluated in vitro, in vivo and for corrosion and wear properties.

Conclusions

The study of phase stability and mechanical properties of binary Ti-Mo and ternary Ti-Mo-Fe alloys using electronic predictive methods was successfully conducted. The X-ray diffraction (XRD) patterns and OM micrographs showed that with increasing *e/a* ratio the β phase stability increased. With increase in stability of β phase, the ultimate tensile strength and elastic modulus decreased from 912 MPa to 540 MPa and 82 GPa to 73 GPa in Alloy A and Alloy B, respectively.

On the other hand, the increase in the β phase stability resulted in increased hardness from 366 $Hv_{0.5}$ for Alloy A to 428 $Hv_{0.5}$ for Alloy B. In agreement with theoretical predictions from *Moeq* and *Bo-Md* methods, the XRD analysis of both alloys displayed only β phase, whereas the *e/a* ratio predicted the presence of α″ and ω phases in Alloy A, which were not detected by XRD although fine substructures were observed from the corresponding OM micrographs. The EBSD phase maps for both Alloy A and Alloy B demonstrated the presence of α″, ω and β phase, where Alloy A revealed high proportion of α″, ω phase which agreed with the phases predicted by *e/a* ratio method as opposed to Alloy B. Therefore, it can be concluded that the theoretical predictive tools were able to provide direction in the design and composition selection in terms of phases likely to form and thus their contribution to overall mechanical properties of each alloy. The addition of low Fe content in Alloy B stabilized the β phase and supressed the presence of α″ phase, resulting in lower elastic modulus as opposed to Ti6Al4V alloy. However, hardness increased significantly with addition of Fe at the expense of strength and elastic modulus, owed to its smaller atomic radius compared to Ti and Mo, thus rendering Fe a strong β stabilizer and solid solution hardener. On the other hand, Alloy A revealed an improved strength compared to Ti-16Mo and Ti-18Mo binary alloys that are reported in literature, thus rendering it a potential material to be considered for use in biomedical applications such as orthopedic implants or vascular stents that requires high strength.

Supplementary Information

The online version contains supplementary material available at https://doi.org/10.1186/s40712-025-00365-x.

Supplementary Material 1.

Acknowledgements

This work was supported and funded by Mintek (Advanced Metallurgy Division) and the studies were funded by CSIR-IBS. The author would like to acknowledge Mintek (AMD) and CSIR (AME and National Laser Center) for providing access to their laboratories. The author thanked colleagues at Mintek (Mr Nelson Molepo and Mr Richard Mathebula) for their assistance with experiments and Mr. Joseph Moema for his support.

Authors' contributions

Nthabiseng Moshokoa: Conceptualization of the manuscript. Nthabiseng Moshokoa, Maje Phasha: Methodology**.** Nthabiseng Moshokoa: Original draft preparation: Nthabiseng Moshokoa, Maje Phasha, Washington Makoana, Lerato Raganya, and Elizabeth Makhatha: Software and Resources**.** Moshokoa Nthabiseng and Maje Phasha: Validation, Formal Analysis, Investigation, Data curation, Reviewing and editing**.** Maje Phasha, Elizabeth Makhatha, Lerato Raganya, Washington Makoana: Supervision**.** Elizabeth Makhatha, and Maje Phasha: Funding acquisition**.** The funders had a role in the design of the study, collection of data, interpretation and analyses of data, in editing the manuscript and in the decision to publish.

Funding

The funders of this work were duly recognised in the acknowledgements.

Data availability

The data that supports the findings of this study will be made available upon request from the corresponding authors (Moshokoa Nthabiseng, Maje Phasha and Elizabeth Makhatha).

Declarations

Competing interests

The authors have no relevant financial or non-financial interests to disclose.

Received: 7 May 2025 / Accepted: 28 October 2025
Published online: 27 November 2025

References

Abd-elrhman Y, Gepreel MAH MAH, Abdel-Moniem A, Kobayashi S (2016) Compatibility assessment of new V-free low-cost Ti–4.7Mo–4.5Fe alloy for some biomedical applications. Mater Des 97:445

Abdel-Hady M, Hinoshita K, Morinaga M (2006) General approach to phase stability and elastic properties of β-type Ti-alloys using electronic parameters. Scripta Mater 55:477

Abdel-Hady Gepreel M, Niinomi M (2013) Biocompatibility of Ti-alloys for long-term implantation. J Mech Behav Biomed Mater 20:407

Abdelrhman Y, Ah M, Kobayashi S, Okano S, Okamoto T (2019a) Biocompatibility of new low-cost (α + β)-type Ti-Mo-Fe alloys for long-term implantation. Mater Sci Eng C Mater Biol Appl 99:552

Abdelrhman Y, Gepreel MAH MAH, Kobayashi S, Okano S, Okamoto T (2019b) Biocompatibility of new low-cost (α + β)-type Ti-Mo-Fe alloys for long-term implantation. Mater Sci Eng C Mater Biol Appl 99:562

Ahmed M, Wexler D, Casillas G, Ivasishin OM, Pereloma EV (2015) The influence of β phase stability on deformation mode and compressive mechanical properties of Ti–10V–3Fe–3Al alloy. Acta Mater 84:124

Akahori T, Niinomi M, Fukui H, Ogawa M, Toda H (2005) Improvement in fatigue characteristics of newly developed beta type titanium alloy for biomedical applications by thermo-mechanical treatments. Mater Sci Eng C Mater Biol Appl 25:248–254

Alves MCR, Rezende (2017) Archives Health Invest 6:458

Alves Rezende MCR, Alves APR, Codaro EN, Dutra CAM (2007) Effect of commercial mouthwashes on the corrosion resistance of Ti-10Mo experimental alloy. J Mater Sci Mater Med 18:154

Arias CF, Herrero MA, Echeverri LF, Oleaga GE, López JM (2018) Bone remodeling: a tissue-level process emerging from cell-level molecular algorithms. PLoS One 13:0204171

Asri RIM, Harun WSW, Samykano M, Lah NAC, Ghani SAC, Tarlochan F, Raza MR (2017) Corrosion and surface modification on biocompatible metals: a review. Mater Sci Eng C Mater Biol Appl 77:1261

Bagariatskii IA, Nosova GI, Tagunova TV (1958) Soviet Phys Doklady 3:1014

Bahl S, Suwas S, Chatterjee K (2021) Comprehensive review on alloy design, processing, and performance ofβtitanium alloys as biomedical materials. Int Mater Rev 66:139

Bălţatu MS, Vizureanu P, Tierean MH, Minciună MG, Achiţei D (2015) Ti-Mo Alloys Used in Medical Applications. Adv Mater Res 1128:111

Bania PJ (1994) Beta titanium alloys and their role in the titanium industry. JOM 46:16

Bhattacharjee A, Varma VK, Kamat SV, Gogia AK, Bhargava S (2006) Metall Mater Trans 37A:1423

Buzatu M, Chica SI, Vasile E, Geanta V, Stefanoiu R, Petrescu MI, Iacob G, Butu M, Sohaciu M (2016) Bull Ser B 78:161

Catanio Bortolano C, Campanelli LC, Mengucci P, Barucca G, Giguère N, Brodusch N, Paternoster C, Bolfarini C, Gauvin R, Mantovani D (2022) J Alloys Compd 925:166757

Cui YW, Wang L, Zhang LC (2024) Towards load-bearing biomedical titanium-based alloys: from essential requirements to future developments. Prog Mater Sci 144:101277

Dal MR, Bó CAF, Salvador MG, Mello DD, Lima GA, Faria AJ, Ramirez R, Caram (2018) Mater Des 160:1186

Davis R, Flower DRF (1979) J Mater Sci 14:712

Furukawa M, Horita Z, Nemoto M, Valiev RZ, Langdon TG (1996) Microhardness measurements and the Hall-Petch relationship in an Al-Mg alloy with submicrometer grain size. Acta Mater 44:4619
Gordin DM, Sun F, Laillé D, Prima F, Gloriant T (2020) How a new strain transformable titanium-based biomedical alloy can be designed for balloon expendable stents. Materialia 10:100638
Guo L, Naghavi SA, Wang Z, Varma SN, Han Z, Yao Z, Wang L, Wang L, Liu C (2022) On the design evolution of hip implants: a review. Mater Des 216:110552
Haghighi SE, Lu HB, Jian GY, Cao GH, Habibi D, Zhang LC (2015) Effect of α″ martensite on the microstructure and mechanical properties of beta-type Ti–Fe–Ta alloys. Mater Des 76:47
Hall O (1951) *Proceedings of the Physical Society* 64, 742
Hanada S, Izumi O (1986) Transmission electron microscopic observations of mechanical twinning in metastable beta titanium alloys. Metall Trans A 17:1409
Hao YL, Niinomi M, Kuroda D, Fukunaga K, Zhou YL, Yang R, Suzuki A (2002) Young's modulus and mechanical properties of Ti-29Nb-13Ta-4.6Zr in relation to α″ martensite. Metall Mater Trans A 33:3137
Ho WF (2008) A comparison of tensile properties and corrosion behavior of cast Ti–7.5Mo with c.p. Ti, Ti–15Mo and Ti–6Al–4V alloys. J Alloys Compd 464:580
Ho W, Ju C, Lin JC (1999) Biomater 20:2115
Hume-Rothery W, Channel Evans KM, Mabbott GW (1934) Philos Trans Royal Soc Lond 233:1097
Ikehata H, Nagasako N, Furuta T, Fukumoto A, Miwa K, Saito T (2004) Phys Rev B Condens Matter Mater Phys 70:1
Ion R, Cabon G, Gordin DM, Ionica E, Gloriant T, Cimpean A (2021) Endothelial cell responses to a highly deformable titanium alloy designed for vascular stent applications. J Funct Biomater 12:33
Molchanova EK, Glazunov SG (1965) *Israel Program for scientific translations*
Jamhari FI, Foudzi FM, Buhari MA, Sulong AB, Radzuan NAM, Muhamad N, Mohamed IF, Jamadon NH, Tan KS (2023) J Mater Res Tech 24:4091
Kobayashi S, Miyamoto A, Okano S, Gepreel MA, Ibrahim M, Ueda M, Ikeda M, Nakai K, Sakamoto T (2014) Mater Sci Forum 783:1280
Kolli RP, Devaraj A (2018) A review of metastable beta titanium alloys. Metals 8:506
Kuroda D, Niinomi M, Morinaga M, Kato Y, Yashiro T (1998) Design and mechanical properties of new β type titanium alloys for implant materials. Mater Sci Eng A 243:244
Laheurte P, Prima F, Eberhardt A, Gloriant T, Wary M, Patoor E (2010) Mechanical properties of low modulus <mml:math xmlns:mml="http://www.w3.org/1998/Math/MathML" altimg="si14.gif" display="inline" overflow="scroll"><mml:mi>β</mml:mi> </mml:math> titanium alloys designed from the electronic approach. J Mech Behav Biomed Mater 3:565
Lee CM, Ju CP, Chern JH, Lin (2002) J Oral Rehabil 29:314
Lee SH, Todai M, Tane M, Hagihara K, Nakajima H, Nakano T (2012) Biocompatible low Young's modulus achieved by strong crystallographic elastic anisotropy in Ti–15Mo–5Zr–3Al alloy single crystal. J Mech Behav Biomed Mater 14:48
Li CL, Mi WJ, Ye SX, Hui Y, Yu WQ (2013a) J Alloys Compd 550:23
Li C, Lee DG, Mi X, Ye W, Hui S, Lee Y (2013b) Phase transformation and age hardening behavior of new Ti–9.2Mo–2Fe alloy. J Alloys Compd 549:152
Li M, Min X, Ye F, Li P, Cheng C, Zhao J (2019) First-principles study of phase stability and elastic properties in metastable Ti-Mo alloys with cluster structure. Mol Simul 45:26
Liang S (2020) Review of the design of titanium alloys with low elastic modulus as implant materials. Adv Eng Mater 22:2000555
Lin DJ, Lin JHC, Ju CP (2002) Structure and properties of Ti–7.5Mo–xFe alloys. Biomaterials 23:1723
Liu Y, Chen LF, Tang HP, Liu CT, Liu B, Huang BY (2006) Design of powder metallurgy titanium alloys and composites. Mater Sci Eng A 418:25
Luo S, Castany P, Thuillier S (2019) Microstructure, thermo-mechanical properties and Portevin-Le Chatelier effect in metastable β Ti-xMo alloys. Mater Sci Eng A 756:70
Min XH, Emura S, Nishimura T, Tsuchiya K, Tsuzaki K (2010) Microstructure, tensile deformation mode and crevice corrosion resistance in Ti–10Mo–xFe alloys. Mater Sci Eng A 527:5506
Min X, Emura S, Zhang L, Tsuzaki K, Tsuchiya K (2015) Improvement of strength–ductility tradeoff in β titanium alloy through pre-strain induced twins combined with brittle ω phase. Mater Sci Eng A 646:279
Morinaga M (2016) Alloy design based on molecular orbital method. Mater Trans 57:213
Morinaga M, Yukawa N, Adachi H (1986) Tetsu-to-Hagane 76:562
Moshokoa NA, Raganya ML, Machaka R, Obadele BA, Makhatha ME (2022) Microstructure and bending properties of solution-treated Ti-Mo binary alloys for biomedical applications. MATEC Web Conf 370:03014
Moshokoa NA, Raganya ML, Machaka R, Makhatha E, Obadele BA (2024) The influence of solution treatment on the phase evolution and tensile properties of binary Ti-Mo alloys. J S Afr Inst Min Metall 124:253
Mostafa D, Abdelrhman Y, Kobayashi S, Omar S, Gepreel M (2025) Low-cost bio-innovative titanium alloys for dental implant approaches (a comparative in vitro – in vivo animal study). Egypt Dent J 71:2303
Nakai M, Niinomi M, Zhao X, Zhao X (2011) Self-adjustment of Young's modulus in biomedical titanium alloys during orthopaedic operation. Mater Lett 65:688
Niu J, Guo Y, Li K, Liu W, Dan Z, Sun Z, Chang H, Zhou L (2021) Improved mechanical, bio-corrosion properties and in vitro cell responses of Ti-Fe alloys as candidate dental implants. Mater Sci Eng C Mater Biol Appl 122:111917
Okazaki Y, Rao S, Ito Y, Tateishi T (1998) Corrosion resistance, mechanical properties, corrosion fatigue strength and cytocompatibility of new Ti alloys without Al and V. Biomaterials 19:1197
Okulov IV, Okulov AV, Soldatov IV, Luthringer B, Willumeit-Römer R, Wada T, Kato H, Weissmüller J, Markmann J (2018) Open porous dealloying-based biomaterials as a novel biomaterial platform. Mater Sci Eng C Mater Biol Appl 88:103
Oliveira NTC, Guastaldi AC (2009) Electrochemical stability and corrosion resistance of Ti–Mo alloys for biomedical applications. Acta Biomater 5:405
Oliveira NTC, Aleixo G, Caram R, Guastaldi AC (2007) Mater Sci Eng A 452:727
Raganya L, Moshokoa N, Obadele B, Makhatha E, Machaka R (2021) Microstructure and mechanical properties of Ti-Mo-Nb alloys designed using the cluster-plus-glue-atom model for orthopedic applications. Int J Adv Manuf Technol 115:3053
Rao GA, Srinivas M, Sarma DS (2006) Mater Sci Eng A 435:84
Ruzic J, Emura S, Ji X, Watanabe I (2018) Mo segregation and distribution in Ti–Mo alloy investigated using nanoindentation. Mater Sci Eng A 718:55
Sabeena M, Murugesan S, Anees P, Mohandas E, Vijayalakshmi M (2017) Crystal structure and bonding characteristics of transformation products of bcc β in Ti-Mo alloys. J Alloys Compd 705:769
Sakaguchi N, Niinomi M, Akahori T, Takeda J, Toda H (2005) Relationships between tensile deformation behavior and microstructure in Ti–Nb–Ta–Zr system alloys. Mater Sci Eng C Mater Biol Appl 25:363
Samimi P, Liu Y, Ghamarian I, Collins PC (2014) A novel tool to assess the influence of alloy composition on the oxidation behavior and concurrent oxygen-induced phase transformations for binary Ti–xMo alloys at 650°C. Corros Sci 89:295
Sandlöbes S, Korte-Kerzel, Raabe D (2019) Mater Sci Eng A 748:312
Song Y, Xu DS, Yang R, Li D, Wu WT, Guo ZX (1999) Theoretical study of the effects of alloying elements on the strength and modulus of β-type bio-titanium alloys. Mater Sci Eng A 260:269
Sun F, Zhang JY, Marteleur M, Gloriant T, Vermaut P, Laille D, Castany P, Curfs C, Jacques PJ, Prima F (2013) Investigation of early stage deformation mechanisms in a metastable β titanium alloy showing combined twinning-induced plasticity and transformation-induced plasticity effects. Acta Mater 61:6406
Tathe A, Ghodke M, Nikalje AP (2010) Inter J Pharma Sci 2:19
Tiwari GP, Ramanujan RV (2001) Review the relation between the electron to atom ratio and some properties of metallic systems. J Mater Sci 36:271
Todros S, Todesco M, Bagno A (2021) Biomaterials and their biomedical applications: from replacement to regeneration. Processes 9:1949
Wang CH, Yang CD, Liu M, Li X, Hu PF, Russell AM, Cao GH (2016) Martensitic microstructures and mechanical properties of as-quenched metastable β-type Ti–Mo alloys. J Mater Sci 51:6896
Wang HL, Hao YL, He SY, Li T, Cairney JM, Wang YD, Wang Y, Obbard EG, Prima F, Du K, Li SJ, Yang R (2017) Elastically confined martensitic transformation at the nano-scale in a multifunctional titanium alloy. Acta Mater 135:330
Xu W, Yu A, Lu X, Tamaddon M, Ng L, dilawer Hayat M, Wang M, Zhang J, Qu X, Liu C (2020a) Synergistic interactions between wear and corrosion of Ti-16Mo orthopedic alloy. J Mater Res Technol 9:10003
Xu W, Chen M, Lu X, Zhang DW, Singh HP, Jian-Shu Y, Pan Y, Qu XH, Liu CZ (2020b) Effects of Mo content on corrosion and tribocorrosion behaviours of Ti-Mo orthopaedic alloys fabricated by powder metallurgy. Corros Sci 168:108557
Zhang LC, Chen LY (2019) A review on biomedical titanium alloys: recent progress and prospect. Adv Eng Mater 21:1801215
Zhao M, Niinomi M, Nakai J, Hieda (2012a) Acta Biomater 8:1990
Zhao X, Niinomi M, Nakai M, Hieda J (2012b) Development of new titanium-molybdenum alloys with changeable Young's modulus for spinal fixture devices. J Solid Mech Mater Eng 6:700

Zhao J, Liu K, Ding M, Yin L, Liang S (2022) Relationship between the composition and elastic modulus of TiZrTa alloys for implant materials. Metals 12:1582
Zhou YL, Luo DM (2011) Microstructures and mechanical properties of Ti–Mo alloys cold-rolled and heat treated. Mater Charact 62:931
Zhou YL, Niinomi M (2009) Ti–25Ta alloy with the best mechanical compatibility in Ti–Ta alloys for biomedical applications. Mater Sci Eng C Mater Biol Appl 29:1061
Zhou YL, Niinomi M, Akahori T, Fukui H, Toda H (2005) Corrosion resistance and biocompatibility of Ti–Ta alloys for biomedical applications. Mater Sci Eng A Mater Struct Prop Microstruct Process 398:28
Żrodowski Ł, Wroblewski R, Choma T, Moronczyk B, Ostrysz M, Leonowicz M, Lacisz W, Blyskun P, Wrobel JS, Cieslak G, Wysocki B, Zrodowski C (2021) K Pomian Mater 14:2541

Publisher's Note